2−10

Numerical Simulations of High Enthalpy Flow

by
Nobuhiro SEKINO, Toru SHIMADA and Naoki TAMURA
Aerospace Division , Nissan Motor Co., LTD.

ABSTRACT

Eleven results of ours to the problems of the 13th NAL Symposium on Aircraft Computation Aerodynamics - High Enthalpy Flow Workshop are presented. The problems are the simulation of flow around a sphere (problem I) and the simulation of flow around the re-entry vehicle, OREX (problem II). To perform these simulations, three kinds of numerical codes for different gas properties are used; for thermo-chemically non-equilibrium gas, for equilibrium gas, and for frozen (ideal) gas. In these codes, Navier-Stokes equations are discretized in the finite volume form using Harten-Yee type TVD flux estimation and LU-SGS implicit method. For the thermo-chemically non-equilibrium flow, eleven chemical species are considered and Park's two temperature model is adopted. The computed heat fluxes for the sphere case agree well with the experimental data provided by the workshop organizer. As for the OREX case, although the computed heat fluxes are somewhat larger than the flight data, the computational results agree with the flight data in the same order. For the particular flow conditions in the case of sphere, our results show that the heat fluxes to the non-catalytic walls are larger than those to the fully-catalytic walls. It is shown that one of the causes for this phenomenon is rapid recombination rate of chemical spices.

1. Introduction

Re-entry vehicles experience severe thermal circumstances during their atmospheric re-entry. Owing to recent progress of computer power, it is realized to simulate such hypersonic flowfields and to evaluate physical values by CFD. In the high enthalpy flow workshop, the CFD performance for this problem is compared by applicants. We use several in-house numerical codes to solve given hypersonic flow problems.

In the following sections, after the discussion of the flow models and numerical methods , some of our results are presented.

2. Numerical Models

2.1 Flow models

The flows around re-entry vehicles vary depending on the flight altitude and velocity. Because of the strong shock waves formed in front of vehicles, the dissociation and the ionization of air may occur. The chemical reaction process may change the flow features such as the shock standoff distance.

Non-equilibrium processes occur in a flow when the time scale required for a process to accommodate itself to local conditions is of the same order as the transit time scale across the considered region. If the accommodation time scale is very short compared with the transit time scale, the process is considered as equilibrium. On the other hand, if the accommodation time scale is very long compared with the transit time scale, the process is frozen.

Three kinds of numerical codes have been developed in our group. They are codes for the thermo-chemically non-equilibrium flow, for the equilibrium flow, and for the frozen flow. Usually one of them is used to simulate a hypersonic flow depending on a problem.

2.2 Thermo-chemically non-equilibrium flow

The approach employed in our code to the thermo-chemically non-equilibrium flow is a two-temperature thermal model proposed by Park. As the chemical species, following 11 species, namely N, O, N_2, O_2, NO, N^+, O^+, N_2^+, O_2^+, NO^+ and e^-, are considered. Therefore the modeled system includes 11 species continuity equations, 3 momentum equations, and 2 energy equations describing the conservation of vibrational-electronic and total energies.

The mass rate of production of each species is expressed by Park's chemical kinetic model. This model includes totally 43 reactions of 21 kinds.

A Landau-Teller model is used to determine the vibrational-translational relaxation process, in which the relaxation rate is proportional to the deviation from the equilibrium state. Millikan and White [1] presented semiempirical formula for estimation of vibrational relaxation time. For

temperatures above 8000 K, Park [2] proposed correction for the vibrational relaxation time, so called collision limiting. We use above two models (Millikan & White's model + Park's collision limiting) to estimate vibrational relaxation time.

As the chemical-vibrational coupling model, the preferential dissociation and recombination model is used. In this model, the dissociation of molecular species is assumed to occur preferentially when the molecules are vibrationally excited. To put it in the concrete, the rate-controlling temperature of dissociation is evaluated by the geometrical average of the local translational-rotational temperature (T_{tr}) and the vibrational-electronic temperature (T_v). If one assumes preferential dissociation and recombination of molecules in the higher vibrational states, the vibrational energy of diatomic molecules, which are created or destroyed, should be larger than the average vibrational energy. This effect is also included in the code.

The transport coefficients are estimated by an extension of Yos's formula to the multi-temperature gas mixture.

Most part of the mathematical model is based on the paper by Gnoffo et. al. [3]

2.3 Wall catalytic effect

For the chemically non-equilibrium flow, results vary according to wall catalytic effects. Generally, we assume the wall catalycity to be fully catalytic or non-catalytic. For the fully catalytic wall, we assume the composition of air at the wall to be equilibrium one that is characterized by the local wall pressure and temperature. For the non-catalytic wall , we set the normal derivative of concentration of each species to the wall to be zero.

2.4 Equilibrium and frozen flow

The procedures to simulate the equilibrium flow and the frozen flow are almost the same. The difference between them is the treatments of the thermodynamic relations. For the frozen air model, the thermodynamic relations are expressed by the ideal gas equation of state. On the other hand, for the equilibrium air model the thermodynamic relations can not be expressed by simple formula. We use curve-fit for the thermodynamic and transport properties [4,5] in simulations of equilibrium flows.

3. Numerical methods

3.1 Discretization in space

The governing equations are expressed in a generalized curvilinear coordinate system and discretized in a finite volume form. We use a structured grid system.

3.2 Flux estimation

To estimate the convective flux term, the Harten-Yee's method [4] extended to the real gas is used. This method is consists of the central difference term and the additional correctional term, with which 2nd-order numerical flux preserving the TVD characteristics is obtained. As the limiter function, we use conventional minmod function.

As for the viscous, thermal conduction, and diffusion terms, the central difference method is used.

3.3 Time integration

To obtain a steady state solution as a time asymptotic one, we use the LU-SGS method [7]. In this method, using the lower-upper symmetric Gauss-Seidel (LU-SGS) factorization, the scalar calculations in forward/backward sweeping are performed instead of the matrix inversion. It is expected that the computational cost can be much reduced with this method.

In the case of the chemically non-equilibrium flow, because of the rapid production rate of species, sometimes the governing equations become stiff. To reduce the stiffness, the point-implicit method is used. In this method, the source term is treated implicitly apart from the convective terms.

3.4 Heat flux estimation

The heat flux to the wall is evaluated by the following expression:

$$\dot{q} = \eta \frac{\partial T_{tr}}{\partial n} + \eta_v \frac{\partial T_v}{\partial n} + \rho \sum_{s=1}^{11} h_s D_s \frac{\partial y_s}{\partial n} \qquad (1)$$

where $\dot{q}$ is the heat flux to the wall, T_{tr} the translational-rotational temperature, T_v the vibrational-electronic temperature, ρ the density, η and η_v the thermal conductivity, h the enthalpy, D the diffusion coefficient, and y the mole fraction, respectively. The normal derivative to the wall is denoted by $\partial/\partial n$. The subscript s represents a species. In the case of non-catalytic wall, the third term in the right-hand side of the equation (1) is zero.

4. Applied cases

In table I, the cases that we have applied in this workshop are summarized. We have performed the computations on the 11 cases of two problems.

Table I Applied cases

Problem	Case	Non-equilibrium		Equilibrium	Frozen
		Non-cat	Full-cat		
I Sphere	1	●			
	2		●		
	3	●			
	4		●		
	5	●			
	6		●		
II OREX	1	●			
	2	●			
	3		●		
	4			●	
	5				●

5. Problem I

Problem I treats flows around a sphere of 40 mm in diameter, where axisymmetric laminar flows are assumed. Computations are performed for 6 cases which include three kinds of main flows and two kinds of wall conditions.

5.1 Computational Grid

In figure 1, the computational grid used in this problem is shown. The number of grid points is 51×81 and the minimum grid spacing near the wall is 2.0×10^{-3} mm.

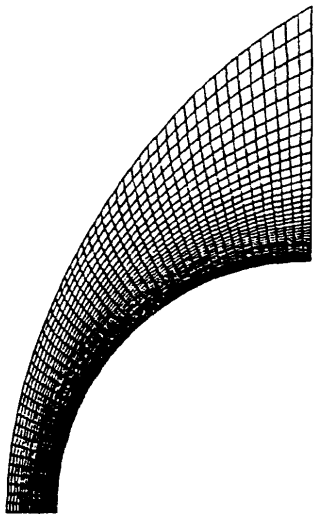

Figure 1 Computational grid for problem I

5.2 Results

Figure 2 shows the pressure contours of cases 1, 3 and 5 respectively. As for cases 2, 4, and 6, almost the same pressure contours are obtained. In these figures, sharp shock waves are captured with no unphysical oscillations.

In figure 3, the temperature distributions along the stagnation streamlines are shown. In these figures, T_{tr} and T_v denote the transrational-rotational temperature and vibrational-electronic temperature, respectively. The horizontal axes in these figures represent the non-dimensional distance from the stagnation point normalized by the maximum length of the computational domain along the axis (in our

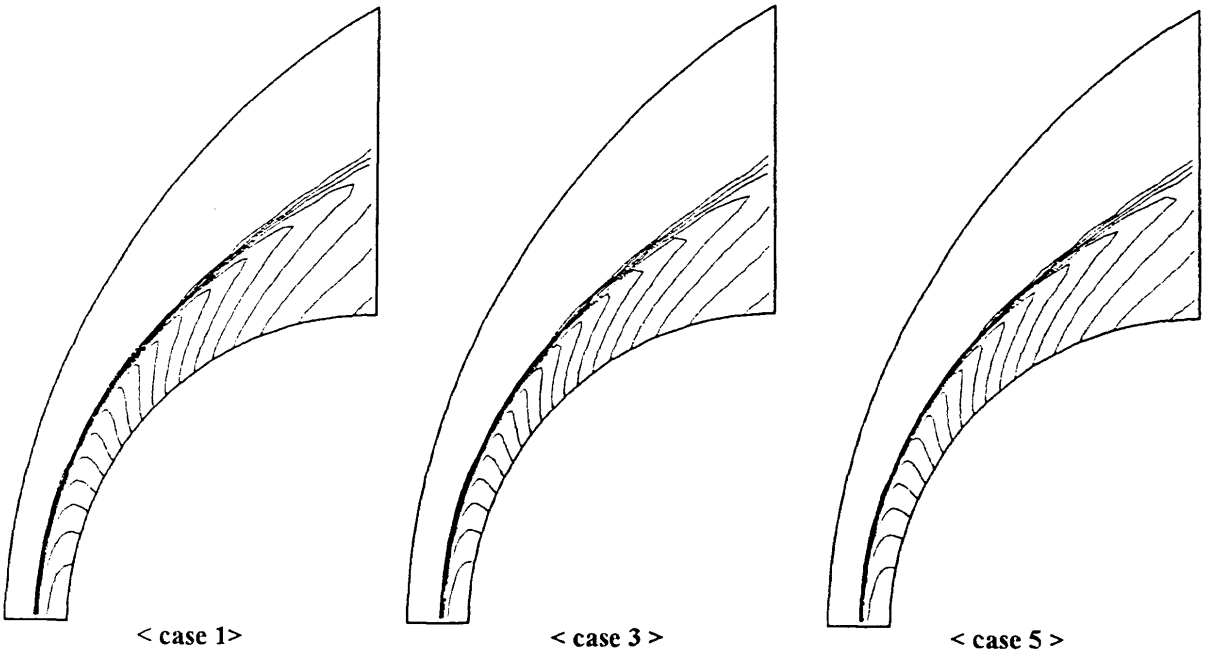

< case 1> < case 3 > < case 5 >

Figure 2 Pressure contours (problem I)

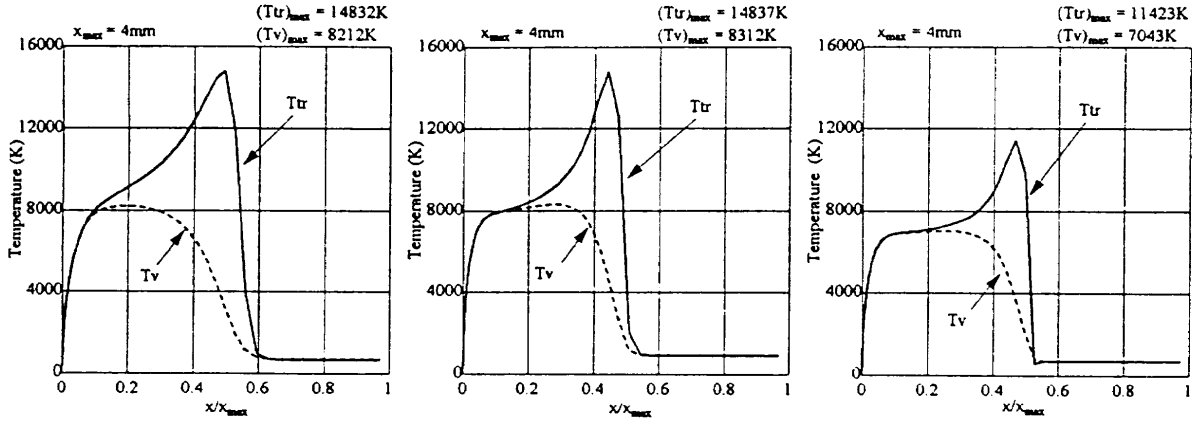

Figure 3 Temperature distributions along the stagnation streamline

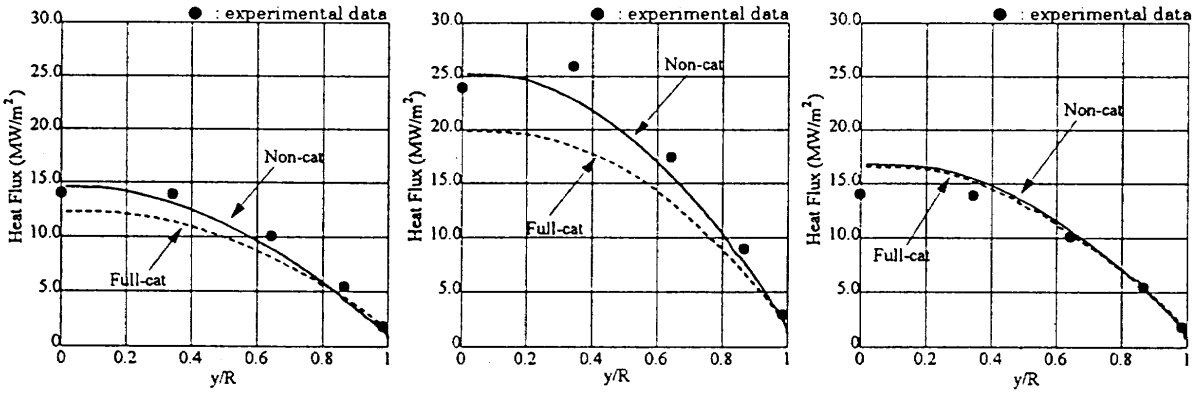

Figure 4 Heat flux distributions along the body surface

case x_{max} = 4 mm). In case 1 it can be seen that the relaxation between T_{tr} and T_v is relatively slow and the non-equilibrium effect seems to be large. On the other hand, in case 5 the relaxation between the two energies seems to be faster than those of the other cases and it is expected that the non-equilibrium effect in this case is relatively small.

Figure 4 shows the heat flux distributions along the body surface. The horizontal axes in these figures represent the non-dimensional distance from the axis line normalized by the sphere radius. In comparison with the results of cases 5 and 6, the heat flux to the non-catalytic wall and fully catalytic wall are almost the same. This fact suggests that the flows of these cases can be considered in equilibrium.

The symbols in these figures represent the experimental results of the wind tunnel tests provided by the workshop organizer. The experimental data agree well with the computed results of non-catalytic wall case. The detail of the test condition is not available, but according to the paper [8] the Teflon coated calorimeter shows non-catalytic behavior.

Usually, it is said that heat flux to a fully catalytic wall is larger than that to a non-catalytic wall under the same flow condition. But contrary to our expectations, in our computed results, heat fluxes to the non-catalytic walls are larger than those of the fully catalytic walls. We will consider this subject in detail in the following section.

5.3 Detail of the heat flux distribution

In figure 5, the calculated heat flux distributions of cases 3 and 4 are shown similarly as in figure 4. In addition to these, the conductive part of heat flux to the fully catalytic wall is shown in figure 5. Figure 6 is taken from the Fay & Riddell's paper [9] and this figure shows the heat flux variation with the recombination rate. The important points in this figure are the reduction of heat transfer to a non-catalytic wall and the fact that a conductive part of heat flux to a catalytic wall is smaller than a heat flux to a non-catalytic wall. The same tendency can be observed in figure 5.

Figure 7 shows the mole fraction along the stagnation streamline. This figure is a close view near the wall. The solid lines in this figure represent the

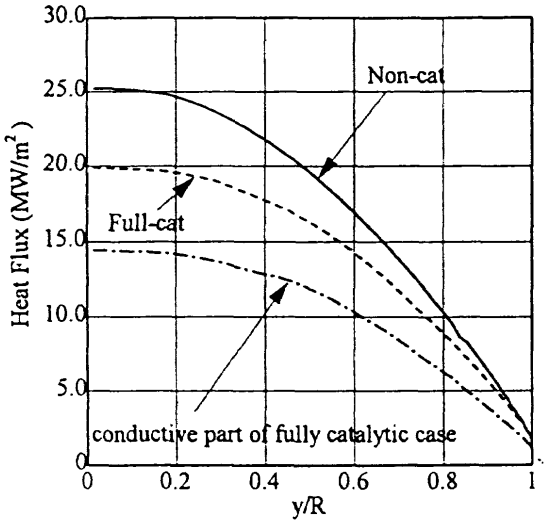

Figure 5 Detail of the heat flux (case 3, 4)

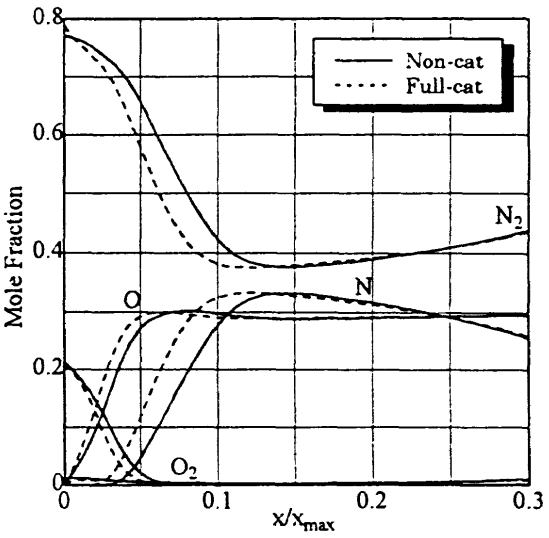

Figure 7 Mole fraction along the streamline (case 3, 4)

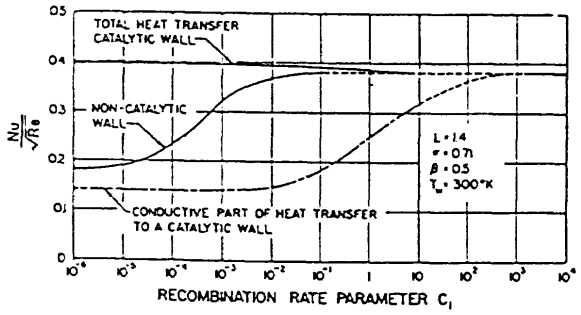

Figure 6 Heat flux variation with the recombination rate (*from Fay & Riddell, ref. 9*)

non-catalytic case and the doted lines the fully catalytic case. As pointed out in reference 9, in the non-catalytic case, the atoms are dammed up and the greater recombination occurs. As a result, the convective heat flux to the non-catalytic wall becomes larger than that to the fully catalytic wall.

Therefore one of the causes of this phenomenon in which the heat fluxes to the non-catalytic walls are larger than those to the fully catalytic walls seems to be rapid recombination rate.

6. Problem II

Problem II deals with the flows around the re-entry vehicle, OREX. In this problem, an axisymmetric laminar flow is assumed as it is in problem I. Two flow conditions are given, and four kinds of air and wall models are applied for one of them. Therefore, in all, 5 cases of computations have been carried out for this problem.

6.1 Computational grid

Figure 8 shows the computational grid used for the computations of cases 2, 3 and 4. The number of grid points is 58×61. For case 1, because the expansion region at the vehicle shoulder makes the computation difficult, the grid that is cut off at the shoulder is used. For case 5, which is the computation of ideal gas, because a shock formed farther away from a body than other cases, a wider computational region is taken.

6.2 Case 1

In figure 9, the computational results of case 1 are presented. The Knudsen number of this case is about 7×10^{-3}, and because of the rarefaction effect, a rather thick shock wave is formed. Figure 10 shows the temperature distributions along the stagnation streamline. The heat flux along the body surface is shown in figure 11. In figure 11, the flight data is plotted by the symbol. The flight data is somewhat smaller than the computational result.

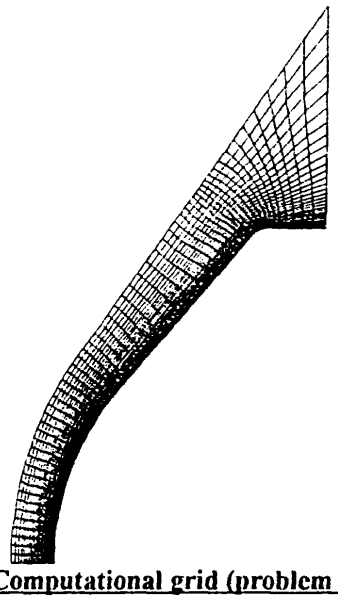

Figure 8 Computational grid (problem II, case 2, 3, 4)

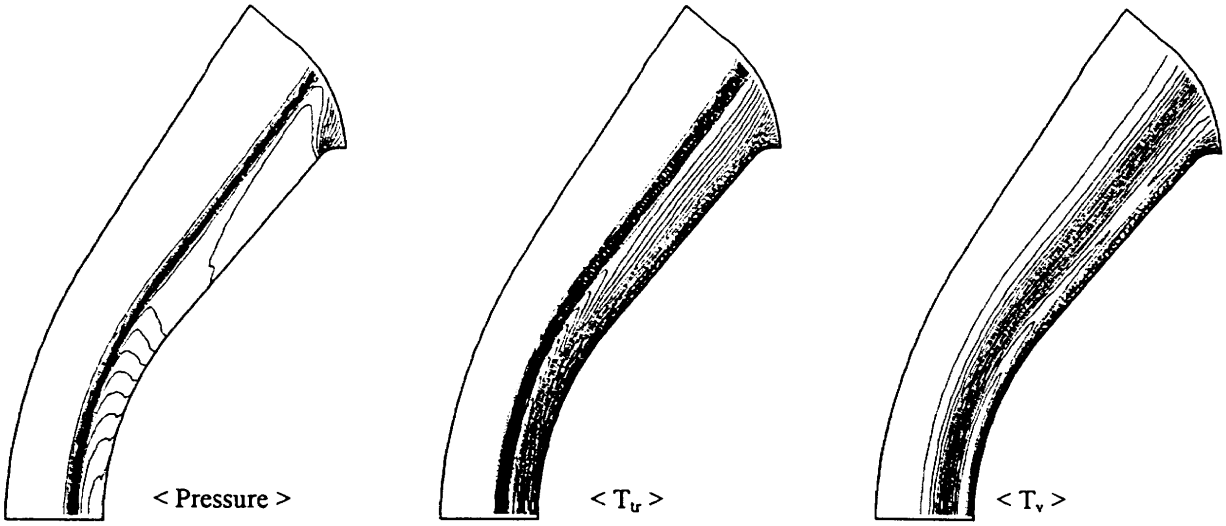

Figure 9 Computational results (Problem II, Case 1)

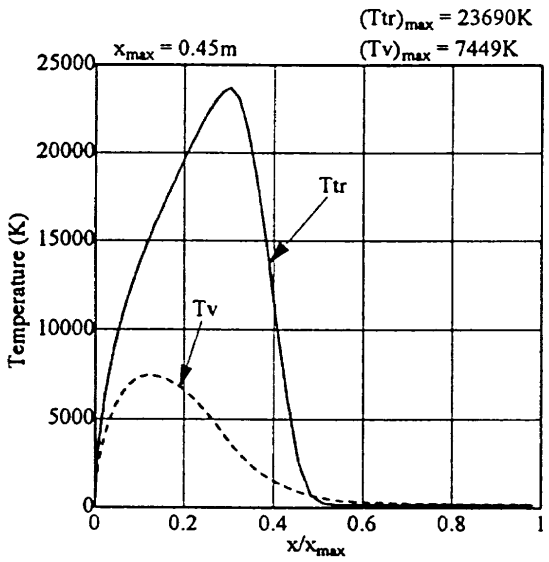

Figure 10 Temperature distributions along the stagnation streamline (problem II, case 1)

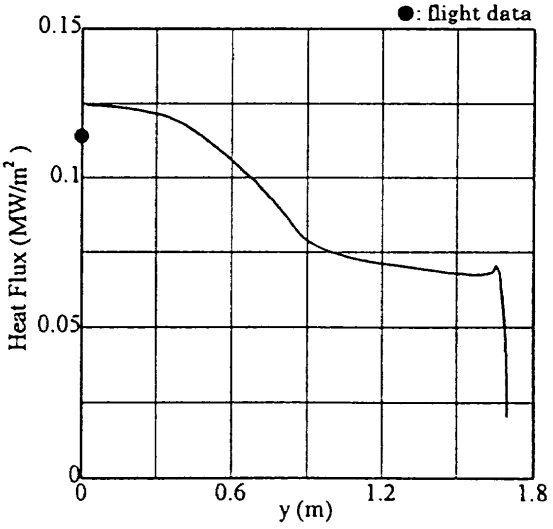

Figure 11 Heat flux distribution along the body surface (problem II, case 1)

6.3 Cases 2, 3, 4 and 5

In problem II, all cases except case 1 are computed under the same flow condition. For cases 2 and 3, the thermo-chemically non-equilibrium flows are assumed. The difference between the cases 2 and 3 is the wall catalytic effect. The non-catalytic wall and the fully-catalytic wall are assumed in cases 2 and 3, respectively. Case 4 is the equilibrium flow case and case 5 is the frozen gas (ideal gas) case. In figure 12, the pressure contours for cases 2, 4, and 5 are shown. Since, in case 5, ideal gas is assumed, the larger shock standoff distance is observed. On the other hand, in case 4 (equilibrium case), because of fast reaction rate, the shock standoff distance becomes the shortest. The heat fluxes to the wall in cases 2, 3, 4 and 5 are summarized in figure 13. For this problem, the heat flux to the fully-catalytic wall is larger than that to the non-catalytic wall. In this figure, the symbol also represents the flight data provided by the workshop organizer. Also in these cases, the computed stagnation heat fluxes are larger than the flight data in some degree.

7. Conclusion

The computations for 11 cases which are our task in "The 13th NAL Symposium on Aircraft Computation Aerodynamics - High Enthalpy Flow Workshop" are described.

In the case of problem I (sphere case), the computed results of non-catalytic wall case agree well with the experimental results. In this problem, the heat fluxes to the non-catalytic walls are larger than those to the fully-catalytic walls. One of the causes of this phenomenon seems to be a rapid recombination

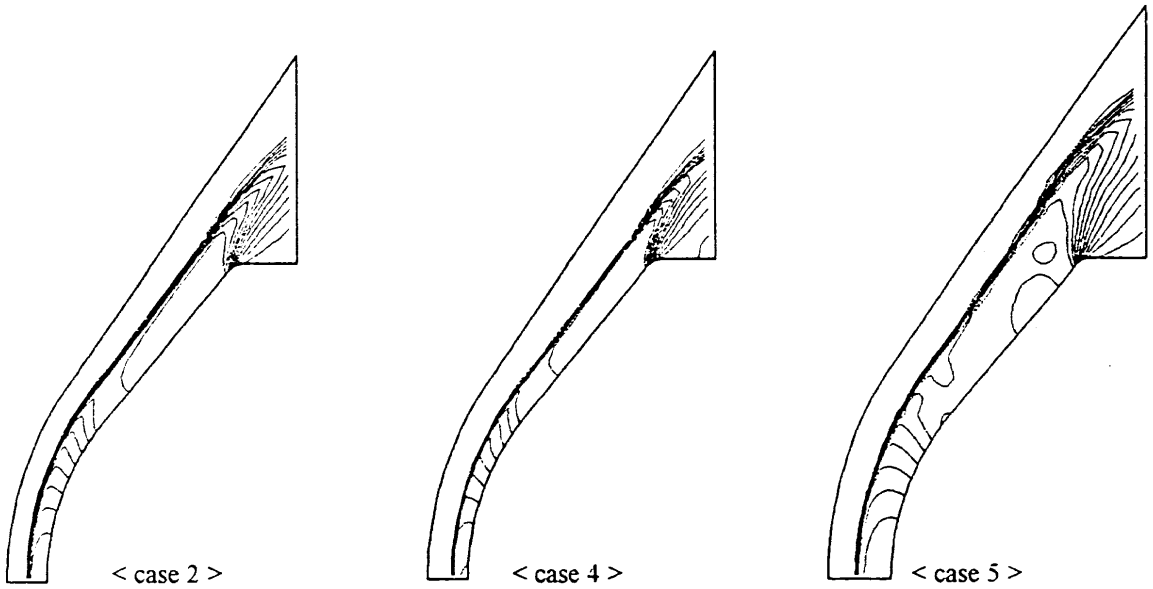

Figure 12 Computational results in the pressure contours (problem II)

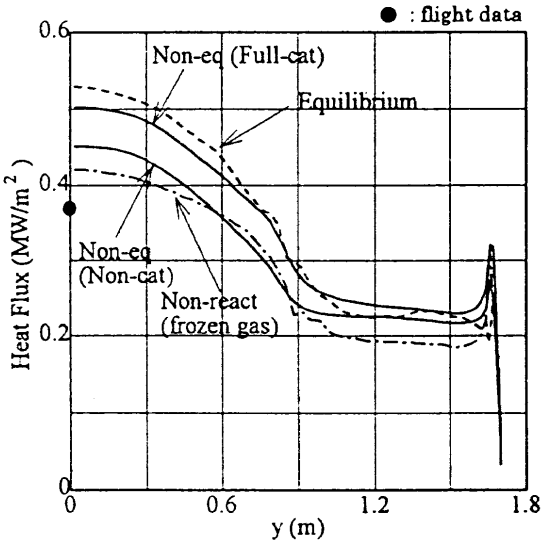

Figure 13 Heat flux distributions along the body surface (problem II, case 2, 3, 4, 5)

rate. More investigation is needed to fully understand this phenomenon.

In problem II (OREX case), the stagnation heat fluxes of two flow conditions are somewhat larger than the flight data, however the computed results agree with the flight data in the same order. In this problem, several computations are performed using different flow models under the common flow conditions. The heat flux distributions do not vary much with the flow model. For the simulation of flight at a high altitude, a thick shock wave is obtained because of rarefaction effect.

It is expected that the demand of space projects which include re-entry may increase and the importance of simulation of high enthalpy flow will be greater and greater. Hereafter we would like to try to develop more sophisticate and effective CFD tools.

References

[1] Millikan, R. C. and White, D. R.; "Systematics of Vibrational Relaxation," J. Chem. Phys., Vol. 39, No. 2, 1963.

[2] Park. C.; "Problems of Rate Chemistry in the Flight Regimes of Aeroassisted Orbital Transfer Vehicles," in *Thermal Design of Aeroassisted Orbital Transfer Vehicles*, H. F. Nelson, ed., Vol. 96 of Progress in Astronautics and Aeronautics, AIAA Inc., 1985.

[3] Gnoffo, P. A., Gupta, R. N. and Shinn, J. L.; "Conservation Equation and Physical Models for Hypersonic Air Flows in Thermal and Chemical Nonequilibrium," NASA-TP-2867, 1989.

[4] Tannehill, J. C. and Mugge, P. H.; "Improved Curve Fits for the Thermodynamic Properties of Equilibrium Air Suitable for Numerical Computation using Time-Dependent or Shock-Capturing methods," NASA-CR-2470, 1974.

[5] Srinivasan, S., Tannehill, J. C. and Weilmuenster, K. J.; "Simplified Curve fits for the Transport Properties of equilibrium Air," ISU-ERI-Ames-88405, 1987.

[6] Yee, H. C. and Harten, A.; "Implicit TVD Schemes for Hyperbolic Conservation Laws in Curvilinear Coordinates," AIAA paper 85-1513, 1985.

[7] Shuen, J. S. and Yoon, S.; "Numerical Study of Chemically reacting Flows Using an LU Scheme," AIAA paper 88-0436, 1988.

[8] Nevin, K. H. and Carroll, F. C.; "Comparative Evaluation of Ablating Materials in Arc Plasma Jets," NASA-CR-1207, 1968.

[9] Fay, J. A. and Riddell, F. R.; "Theory of Stagnation Point Heat Transfer in Dissociated Air," Journal of the Aeronautical Sciences, Vol. 25, No. 2, 1958.